Nanoscopic characterization of type II porous liquid and its use for CO_2 absorption from molecular simulation

Mert Atilhan [a],*, Alberto Cincotti [b], Santiago Aparicio [c],*

[a] *Department of Chemical and Paper Engineering, Western Michigan University, Kalamazoo, MI 49008-5462, USA*
[b] *Department of Mechanical, Chemical and Materials Engineering, University of Cagliari, 09123 Cagliari, Italy*
[c] *Department of Chemistry, University of Burgos, 09001 Burgos, Spain*

ARTICLE INFO

ABSTRACT

The properties of cage(3^3:13^3) macrocycle in perchloropropene (PCP) as model for type II porous liquids were studied using molecular simulation tools. Likewise, the behaviour of CO_2 in these porous liquid phases were studied to analyse the nanoscopic mechanism for carbon capture purposes. Quantum chemistry calculations using Density Functional Theory were carried out to characterize the intermolecular forces between cage, solvent and CO_2 molecules. Molecular dynamics simulations of liquid phases at different cage concentration provides information on the structuring, aggregation, solvation and dynamic properties of these porous liquids. The reported results led to a full characterization of the features controlling type II porous liquids properties as well as the behaviour of carbon dioxide in them, thus providing the required information for the proper design of porous liquids and their use for carbon capturing operations. The nanoscopic structure of the studied fluids showed that it is possible to solubilize suitable amounts of the cages in the solvents to develop a network of pores in the liquid to capture CO_2 in an efficient way.

1. Introduction

Porous liquids are defined as liquid phases containing intrinsic permanent cavities, i.e. pores, and they were firstly considered by James et al. [1]. The requirement of permanent empty spaces into the liquid to be classified as porous leads to three different types: i) type I, neat liquids with intrinsic porosity, ii) type II, liquids formed by the solution of an empty host (cage) into a suitable solvent whose molecules can not penetrate the cage cavity, and iii) framework materials dispersed into a hindered solvent [1,2]. Type II porous liquids have attracted great attention because of the possibility of developing a suitable collection of materials through the design and selection of both cages and solvents, even considering robotic design of suitable cage -solvent combinations [3]. Many of the developed type II porous liquids are based on porous organic cages (POCs), which are molecules with internal cavities being accessible through molecular windows [4]. The first type II based on POCs used crown-ether functionality and was successfully dissolved in 15-crown-5 ether [5]. Dynamic covalent scrambling [5] has proved to be a suitable approach for designing cages to develop type II porous liquids. The use of scrambled cages allows to solve two of the main problems in the development of type II porous liquids: i) a large number of cavities is required for practical purposes, i.e. high solubilities for cages is required,

and ii) cage internal cavities must remain empty, and thus, solvent molecules should not be able to penetrate into the cages (size excluded solvents). Previous studies have showed that two POCs, namely CC3 and CC13 are able to scramble into a cage (3^3:13^3), Fig. 1, with large solubility in perchloropropene (242 mg mL^{-1}), leading to a type II porous liquids with moderate viscosity (11.7 mPa s for a 20% *w/v* solution at 22 °C), which lead to a suitable porous liquid for many different practical applications [6]. Additional cages were designed in the literature starting from this cage (3^3:13^3) through an automatic screening procedure [3].

In literature, one of the main highlighted applications of porous liquids is gas capture purposes, considering that gas selectivity can be controlled through the design and selection of cage windows size [7]. In particular, the CO_2 solubility was considered [6], which is of great relevance for environmental purposes through the development of post-combustion carbon capture operations from flue gases in fossil fuels combustion.

The development of new type II porous liquids requires a detailed knowledge at the nanoscopic level of the main properties of these materials. For this purpose, molecular simulation approach may provide the required characterization, thus contributing to the porous liquid field development. In spite of the relevance of these theoretical studies, the available literature is scarce. Some studies have been reported using molecular dynamics simulations to probe that solvent molecules (like PCP) are excluded from scrambled cages cavities, e.g. cage(3^3:13^{13})

* Corresponding authors.
E-mail addresses: mert.atilhan@wmich.edu (M. Atilhan), sapar@ubu.es (S. Aparicio).
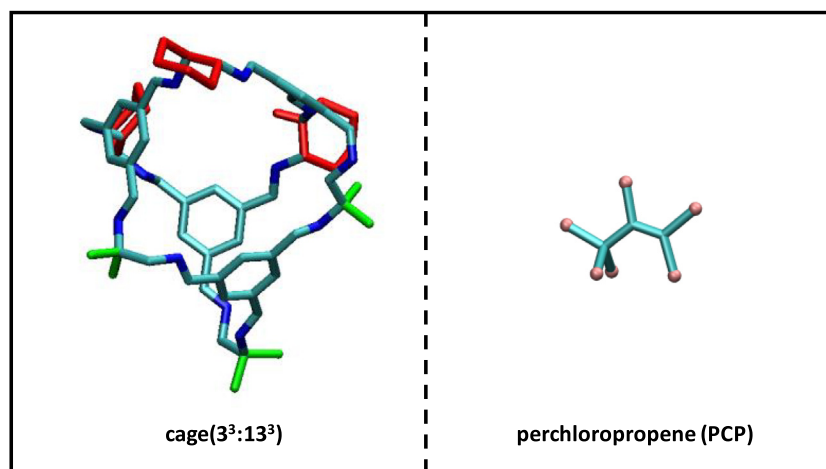
Fig. 1. Porous organic cage and solvent considered in this study for the development of type II porous liquids. Color code: (cyan) carbon, (blue) nitrogen, (red) cyclohexyl rings, (green) dimethyl sites, (pink) chlorine atoms. The reported structures are optimized at B3LYP / 6-311G(d,p) theoretical level.

[6], or to analyse the behaviour of gas molecules, like methane, in these type II porous liquids [5]. Some literature studies have reported Density Functional Theory (DFT) studies on gas sorption by porous liquids. Hollow silica porous ionic liquids for CO_2 absorption were studied by Zhang et al. [8] probing the prevailing role of hydrogen bonding in the structuring of these systems and the interaction with the gas molecules. DFT studies on CO_2 in porous liquids formed by organic cages in PCP were studied by Yin et al. [9], showing gas absorption by the cages through hydrogen bonding and π-π interactions, with the strongest gas – cage interactions inferred for cage(3^3:13^{13}). Additional gases have also been studied in porous liquids by using DFT; Yin et al. [10] studied hollow silica-ionic liquids systems with regard to SO_2 absorption confirming the role of hydrogen bonding and π-hole interactions. Nevertheless, the available nanoscopic information is still scarce and a fully detailed characterization of these systems is required.

This work considers the type II porous liquid formed by cage (3^3:13^{13}) + PCP, at different cage concentrations, with the objective of inferring the main characteristics of the liquid phases in terms of intermolecular interactions, cage solvation, molecular diffusion, and structural properties. The type of cage and solvent were selected according to their suitability [3,5,6], in terms of cage solubility and fluids viscosity, which leads to a representative of type II porous liquids. Likewise, the behaviour of CO_2 absorbed in the same porous liquid was analysed to study the mechanism of gas capture and interaction with the solvent constituents, with the objective of study the nanoscopic features of this material for its possible use for post-combustion carbon capture operations. The computational methodology considers a combined quantum chemistry approach, using DFT, and classical Molecular Dynamics (MD) simulations. The reported results provide a full nanoscopic characterization of type II porous liquids, in neat phases and upon CO_2 absorption, contributing to the development of these promising fluids for technological applications for the first time.

2. Methods

2.1. Density functional theory calculations

DFT calculations were carried out for the isolated monomers (cage (3^3:13^3), PCP and CO_2), as well as for cage(3^3:13^3) – PCP 1:1 dimers and for cage(3^3:13^3) – PCP – CO_2 1:1:1 trimers, using ORCA software [11]. The computational procedure required a two steps process considering the large number of atoms for dimers (156) and trimers (159), to maintain simulation times in a reasonable framework. Therefore, geometry optimizations involved i) first, structures being relaxed using PM3

method, and ii) output structures from PM3 calculations being subjected to further geometry relaxation with the B3LYP functional [12,13], coupled with van der Waals semiempirical contribution described according to the method by Grimme [14], DFT-D3, and 6–311 ++G** basis set.

In the case of cage(3^3:13^3) – PCP 1:1 dimers, six different configurations were considered, namely dimer_PCP_01 to dimer_PCP_06, to explore the main interaction sites. Likewise, for the cage(3^3:13^3) – PCP – CO_2 1:1:1 trimers, six different configurations were studied, namely, trimer_PCP_CO$_2$_01 to trimer_PCP_CO$_2$_07, including CO_2 molecule in the main interaction sites outside the cage as well as the CO_2 molecule confined inside the cage(3^3:13^3) internal cavity.

For all the considered systems, the interaction energy (ΔE) was calculated to quantify the strength of the interactions, being defined as the energy difference between the corresponding multimer and the sum for the corresponding monomers with the Basis Set Superposition Error (BSSE) corrected with the counterpoise method [15]. Atomic charges were calculated according to the ChelpG method [16]. Additional calculations were carried out to infer infrared spectra as well as thermodynamic parameters for the interactions. The topological analysis of the intermolecular forces for the optimized geometries were carried out according to the quantum theory of atoms-in-molecules (Bader's AIM theory) [17] using the Multiwfn program [18]. AIM analysis characterize interactions by so-called critical points, which can be classified as bond, BCP (3,−1), ring, RCP (3,+1), or cage, CCP (3,+3), for which electron density, ρ, and Laplacian (∇) of electron density, $\nabla^2\rho$ [19] are used to quantify the nature and strength [20,21]. Likewise, the use of the Reduced density Gradient analysis (RDG) into the non-covalent interaction (NCI) approach [22] was considered to infer further characterization of the mechanism of interaction.

2.2. Classical molecular dynamics simulations

MD simulations reported in this study were carried out with MDynaMix v.5.2 [23] software using the forcefield parameterizations reported in Table S1 (Supplementary Information). The forcefield parameterizations for the three included molecules (cage(3^3:13^3), PCP and CO_2) were extracted form SwissParam database [24], considering Merck Molecular Force Field [25], except atomic charges which were obtained from DFT / ChelpG calculations of monomers as reported in the previous section.

The studied systems correspond to i) cage(3^3:13^3) + PCP mixtures at three different compositions, and ii) cage(3^3:13^3) + PCP + CO_2 mixture, for a fixed CO_2 content. The number of molecules considered in

each case are reported in Table S2 (Supplementary Information). Initial simulation boxes, corresponding to 1 g cm^{-3} density, were built using PACKMOL [26] program. The objective of these simulations is to understand the behaviour of the porous liquid as a function of cage content as well as the solution of CO_2 to check its suitability for carbon capturing purposes. In the case of cage(3^3:13^3) + PCP mixtures three different compositions were considered with x (cage mole fraction) being 0.035, 0.040 and 0.045, corresponding to 13.1, 14.8 and 16.5 wt%. These concentrations (corresponding to 267, 308 and 345 mg mL^{-1}) are slightly above the reported experimental solubility data (242 mg mL^{-1}) [6] but considering the larger temperature used for MD simulations, they may be considered as reasonably representative systems including enough cages for statistical purposes. In the case of CO_2 + porous liquid mixtures, a mixture with moderate CO_2 content (3.9 mg mL^{-1}) was considered, Table S2 (Supplementary Information).

All MD simulations were carried out in the NPT ensemble at 300 K and 1 bar considering periodic boundary conditions in the three spatial directions. Simulations were carried out in a two stages process: *i*) 10 ns long for equilibration purposes, and *ii*) 100 ns production runs. The equilibration before production runs was assured through the analysis of total potential energy, intermolecular interaction energies and density. Systems pressure and temperature were controlled using the Nose–Hoover method. The Ewald method [27] (15 Å for cut-off radius) was applied the control of electrostatic interactions. Lennard-Jones contributions were calculated with 15 Å cutoff with cross terms calculated using Lorentz-Berthelot mixing rules. The equations of motion were

considered with the Tuckerman–Berne double time step algorithm [28] (1 and 0.1 f. for long and short-time steps). The analysis of results and visualization were carried out with MDynamix – TRANAL [23], VMD [29] and TRAVIS [30] programs.

3. Results and discussion

3.1. DFT results for molecular clusters cage + PCP

The porous liquid formed by cage(3^3:13^3) in PCP should be characterized by the interaction of the solvent (PCP) molecules with the cages structures. For this purpose, DFT calculations were carried out on cage – PCP interactions. Therefore, six different main interaction sites were considered, Fig. 2, and the structures were optimized considering placement of PCP at mentioned positions. These sites were selected considering the main possible gas absorption sites: cage windows, cyclohexyl sites, dimethyl sites as well as cage vertices. The possibility of PCP molecules inside cage internal cavity was also explored, for this purpose a single PCP molecule was initially placed inside the cavity and it was tried to be optimized using DFT. The optimization of PCP inside cage cavity was not possible, which can be attributed to steric hindrance as PCP molecules do not fit inside the cage cavity. Therefore, the discarding of the possible placement of PCP molecules inside the cages confirms that cage – PCP may form true type II porous liquids, i.e. cavities not occupied by solvent molecules. The optimized structures for 1 cage – 1 PCP clusters reported in Fig. 2 show very different strength
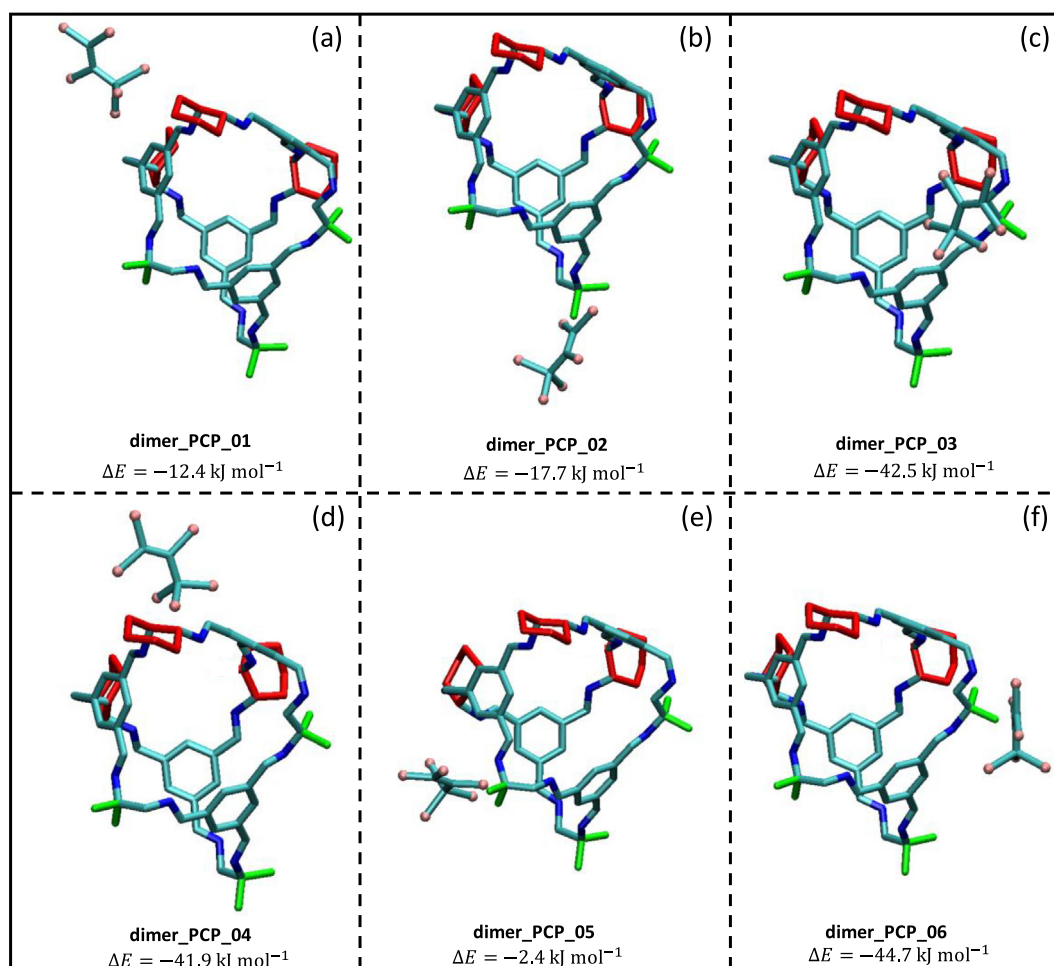

Fig. 2. Optimized structures of cage(3^3:13^3) – PCP dimers for different possible interaction sites, calculated at B3LYP / 6-311G(d,p) theoretical level. Counterpoise corrected interaction energies, ΔE, are reported for each dimer. Color code as in Fig. 1.
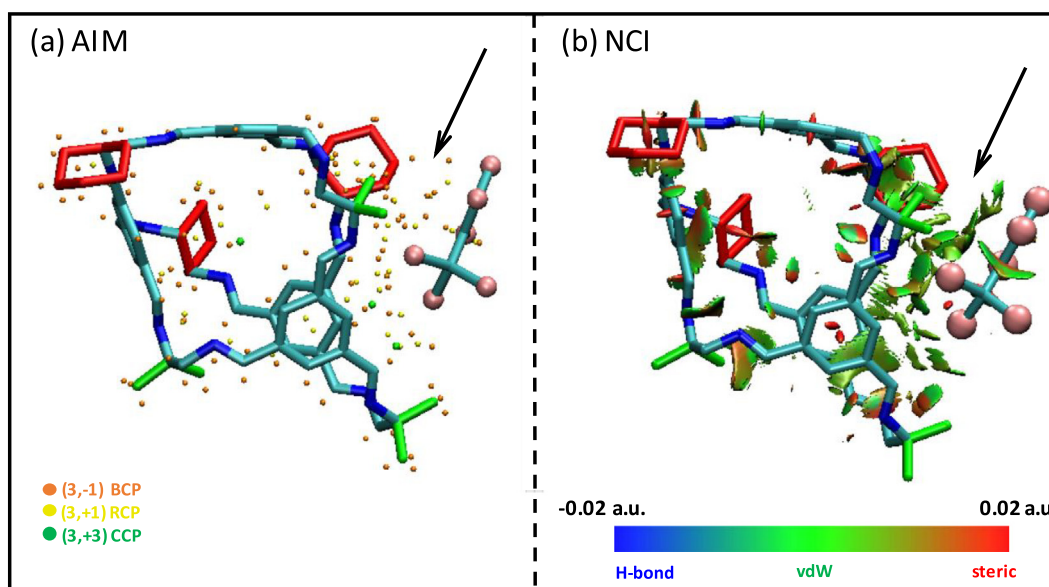
Fig. 3. AIM and NCI analysis of dimer_PCP_06 (Fig. 2) for structure optimized at B3LYP / 6-311G(d,p) theoretical level. Arrows indicate the region for cage(3^3:13^3) – PCP interactions. Dimer labelling as in Fig. 2.

of interaction, quantified using the interaction energy, ΔE, thus being largely dependent on the position of PCP molecule with regard to the cage. Larger ΔE values are obtained in the vicinity of cage windows (Fig. 2c, d and f) whereas remarkably lower values are inferred in on top of the cyclohexyl sites (Fig. 2a) or in the vicinity of the dimethyl sites (Fig. 2b or e). Thus, PCP molecules approaching to the cages would be preferently placed in the cage window region, but without penetrating in the cavity. The reason for the preference for close to cage windows regions may be inferred from AIM and NCI analysis as reported in Fig. 3. PCP molecules may adopt a quasi-planar configuration on top of the cage window leading to a large BCPs and RCPs all along the cage window region, Fig. 3a, which would justify the strength of the interaction reported in Fig. 2f in comparison with the non-window interaction sites. This behaviour is confirmed by the NCI analysis reported in Fig. 3b, which shows a large and continuous region corresponding to van der Waals – like interactions all along the window in the region just below the PCP molecule. Therefore, the PCP – cage intermolecular interaction is characterized by a large number of van der Waals – like contacts, which although not very strong separately, the presence of a large number of these contacts in the cage windows region leads to very effective PCP – cage total interaction, which would be in the roots of the good solubility of the studied cages in this PCP solvent.

The effect of the presence of PCP molecules should change cage properties, which can be calculated to further analyse the PCP – cage interactions. Results in Table 1 show the molecular orbitals HOMO – LUMO gap as calculated for clean cage and for 1 cage – 1 PCP dimers. In all the cases, the interaction of the cage with PCP leads to a decrease in the gap, although those dimers with larger ΔE (03, 05 and 06) lead to lower decrease in the gap (roughly 0.3 eV) in comparison with dimers with lower ΔE (01, 02 and 04) which lead to a decrease in the gap of 0.5–0.6 eV. This interaction of cage with PCP molecule leads to the stabilization of the cage structure but with larger effects in certain positions (close to window regions). Likewise, the possible cage – PCP charge transfer was analysed, and the reported ChelpG charges for PCP molecules upon interaction with the cage are reported in Table 1. Although a minor PCP to cage charge is inferred, with PCP molecules slightly positively charged, this effect is almost negligible for all the considered sites, thus discarding its effect on intermolecular interactions, which are mainly of van der Waals site as inferred for results in Fig. 3.

Additional changes in cage properties by the presence of interacting PCP molecules may be inferred from the calculated IR spectra as reported in Fig. 4. Spectra for clean cage, Fig. 4a, and isolated PCP molecule, Fig. 4b, were calculated and compared with those for the cage – dimer clusters considering two very different interaction sites: *i*) above the cyclohexyl ring (01; Fig. 4c) and *ii*) the largest ΔE site corresponding to window cage (06; Fig. 4d). The reported results show that the main vibrational features of the cage do not suffer remarkable changes upon interacting with PCP molecule. The peak at 3054 cm^{-1} is maintained for dimer 06 and slightly redshifted for dimer 01, whereas the peak at 1718 cm^{-1} is maintained constant for both dimers. The interaction with the cage in dimer 06 is produced in the window region and being of van der Waals character does not lead to remarkable changes in the cage vibrations. In the cage of dimer 01, the interaction is produced through the cyclohexyl sites, which lead to some changes although not very large. Therefore, intermolecular interactions through the window cages maintain most of the vibrations features of the cage. In the case of PCP molecules, the most remarkable peaks, like the one at 742 cm^{-1}, are not changed upon interacting with the cage, thus confirming the nature of the interactions as van der Waals – like with the formation of a large number of these interactions as the reason for the large ΔE, although each interaction (atom to atom) not being very strong, which is especially true for the cage windows region. The molecular orbitals of cage – PCP are reported for cluster 06 in Fig. 5. The HOMO is totally localized in the cage, corresponding to atoms in the cage

Table 1
Properties of cage(3^3:13^3) and cage(3^3:13^3) – PCP dimers calculated at B3LYP / 6-311G (d,p) theoretical level.

dimer	ΔE_G / eV	q_{PCP}
cage(3^3:13^3)	4.70	–
dimer_PCP_01	4.14	0.03
dimer_PCP_02	4.19	0.02
dimer_PCP_03	4.35	0.02
dimer_PCP_04	4.08	0.05
dimer_PCP_05	4.46	0.03
dimer_PCP_06	4.40	0.01

Dimer labelling as in Fig. 2. HOMO-LUMO energy gap (ΔE_G); total ChelpG charge on PCP molecule (q_{PCP}).
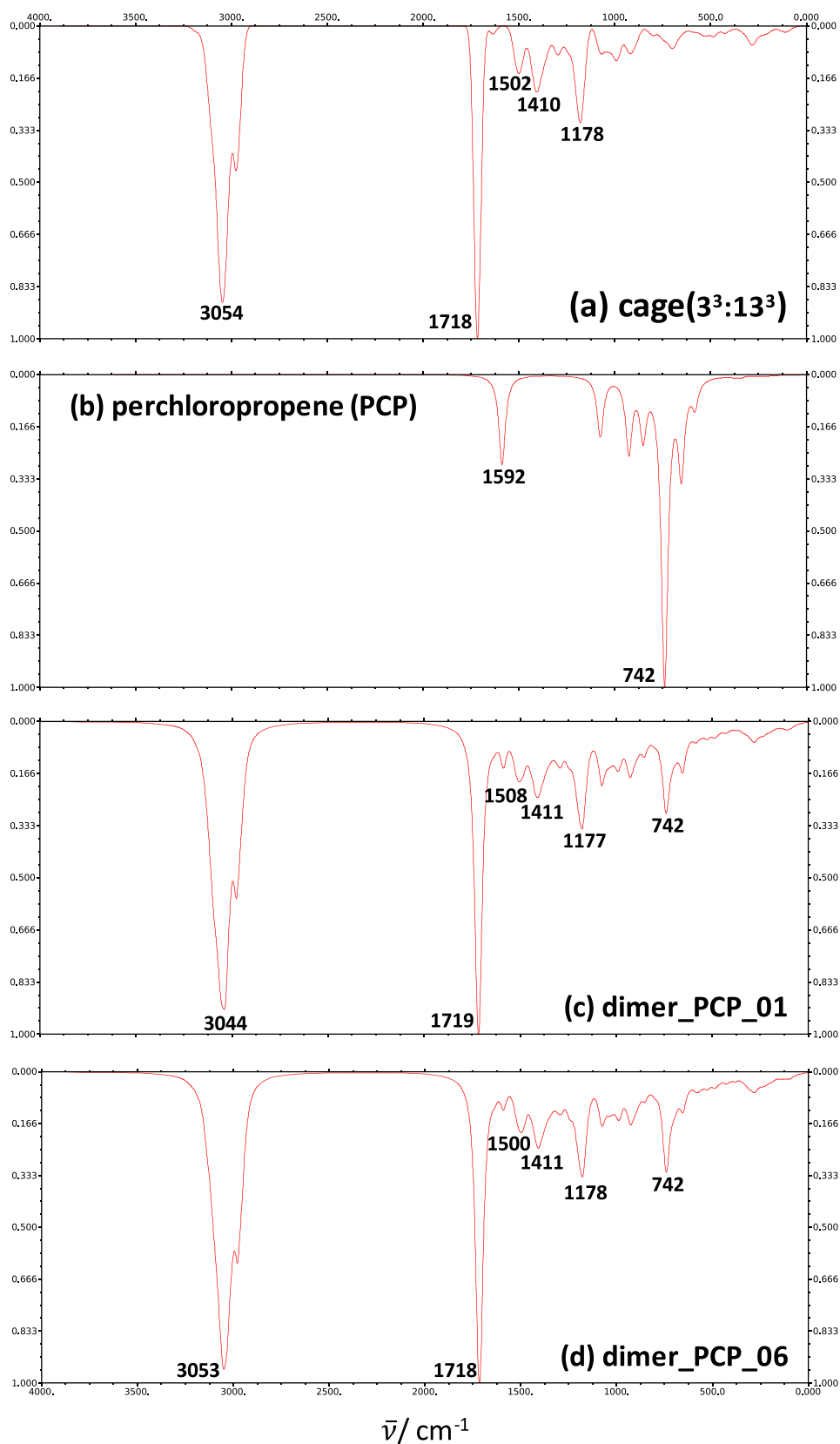
Fig. 4. IR spectra from DFT optimized structures at B3LYP / 6-311G(d,p) theoretical level of (a,b) the reported monomers and (c,d) dimers. Dimers labelling as in Fig. 2. Values inside each panel indicate the most relevant peaks.

windows region, whereas the LUMO is placed in the PCP molecules. The density of states reported in Fig. 5c show the prevalence of cage contribution to the total density of states over PCP, which is especially relevant for the region in the vicinity of the HOMO. This HOMO – LUMO arrangement should affect the electronic properties of the cage upon interaction with the PCP, because of the presence of the first unoccupied orbital in the PCP molecules.

3.2. MD results for cage + PCP liquid mixtures

The MD analysis of the cage – PCP solutions allows to infer additional information to that provided by DFT calculations using small clusters approach. Likewise, the cage concentration effect was also studied using MD. Although DFT results discarded the possibility of having PCP molecules inside the cage cavity, this was also analysed using MD results. Greenaway et al. [6] analysed the distribution of PCP molecules around cage(3^3:13^3) using a geometric criterion around the cage center-of-mass, d: $d \leq 3.5$ Å (inside cage), $d = 5.5$ Å (cage window region), $d = 9.0$ Å (around cage), $d > 9.0$ Å (pseudobulk liquid PCP). Using this geometric criterion the PCP arrangement around the cages was calculated with results in Fig. 6a showing that cages cavities are empty for all the studied concentrations, thus confirming the type II

porous liquid character. There is also a non-negligible number of molecules in the cage windows, increasing with concentration as well as in the close region to the cavity, but with most PCP molecules placed away of the region closely around the cage, Fig. 6a. Although the number of PCP molecules directly interacting with the cages, those in the windows and in the first solvation shell, increases with concentration, this variation is not too large. It should be considered that the size of PCP molecules (139.7 Å^3 calculated molecular volume) is large thus limiting the number of molecules around the cages because of steric hindrance in spite of the large affinity inferred from DFT results. The formation of type II porous liquids should lead to volume expansion upon the addition of cage molecules, this effect was quantified through the so called percentage volume expansion ($\%V^{exp}$) in which the volume of the neat PCP is compared with that of PCP + cage solutions, Fig. 6b. The expansion because of the presence of cage molecules is confirmed and it increases with cage concentration; nevertheless, this effect is moderate, showing that the disruption of PCP liquid structuring because of the cage molecules is not too large, with the solvent being able to arrange its structuring around the solute maintaining most of its properties, with this efficient solvation being on the roots of good cage solubility. To confirm this effect, radial distribution functions, RDFs, for PCP – PCP pairs were calculated for cage – PCP solution and compared
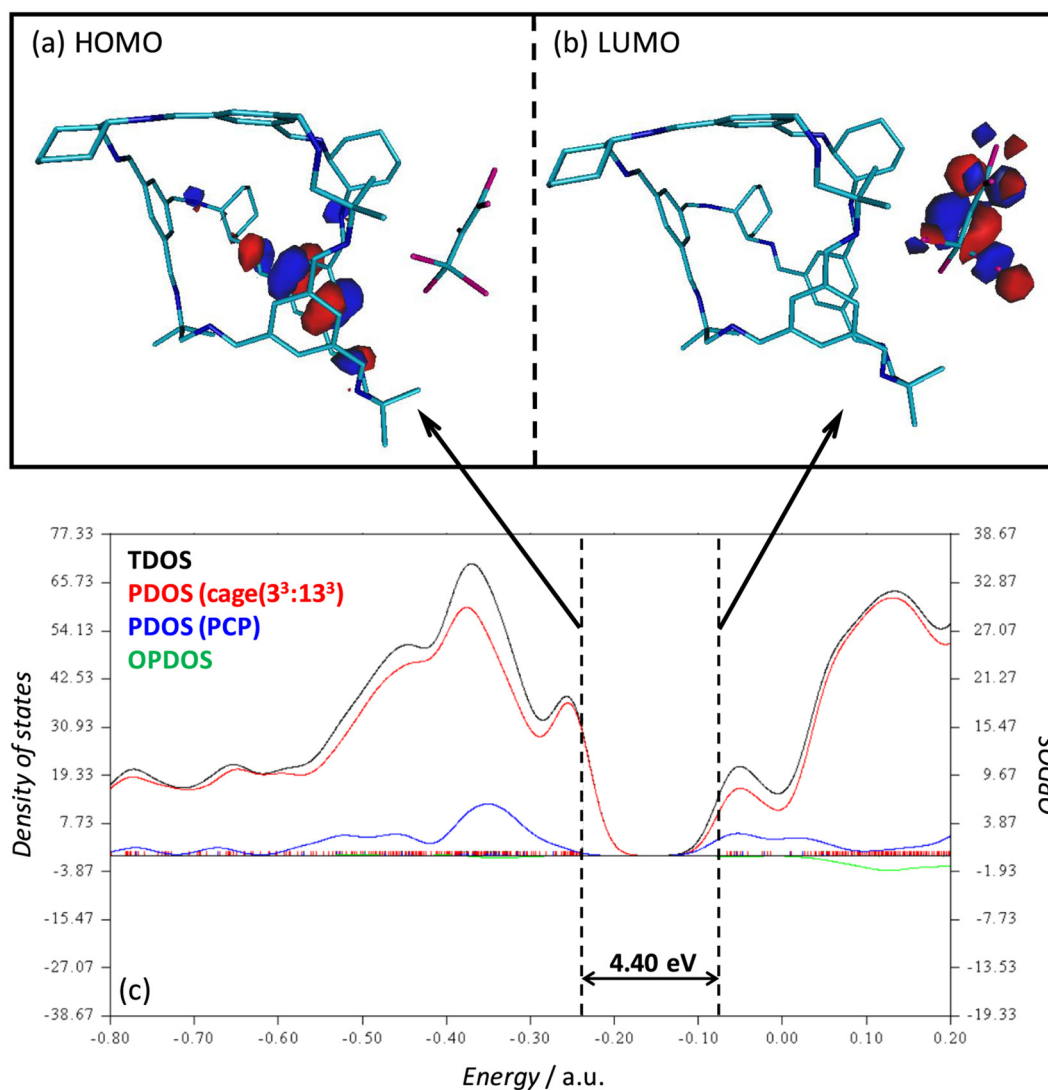

Fig. 5. (a,b) Molecular orbitals (HOMO and LUMO) and (c) the corresponding density of states from DFT optimized structures at B3LYP / 6-311G(d,p) theoretical level of dimer_PCP_06. Dimer labelling as in Fig. 2. In panel c, total density of states (TDOS), partial density of states (PDOS) for the corresponding molecules and overlap density of states (OPDOS) are reported.
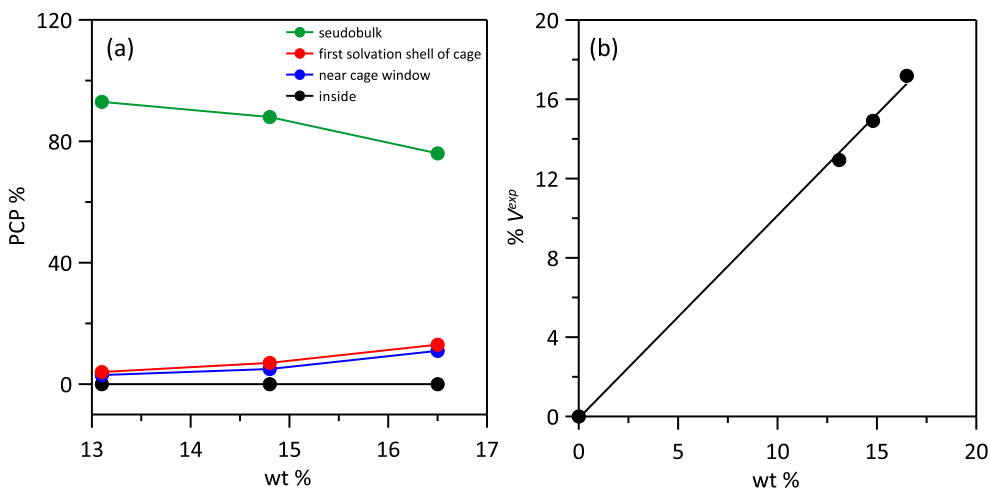
Fig. 6. (a) Cage occupancy and (b) percentage volume expansion, $\%V^{exp}$, for cage(3^3:13^3) + PCP solutions for different cage content from MD simulations at 300 K.
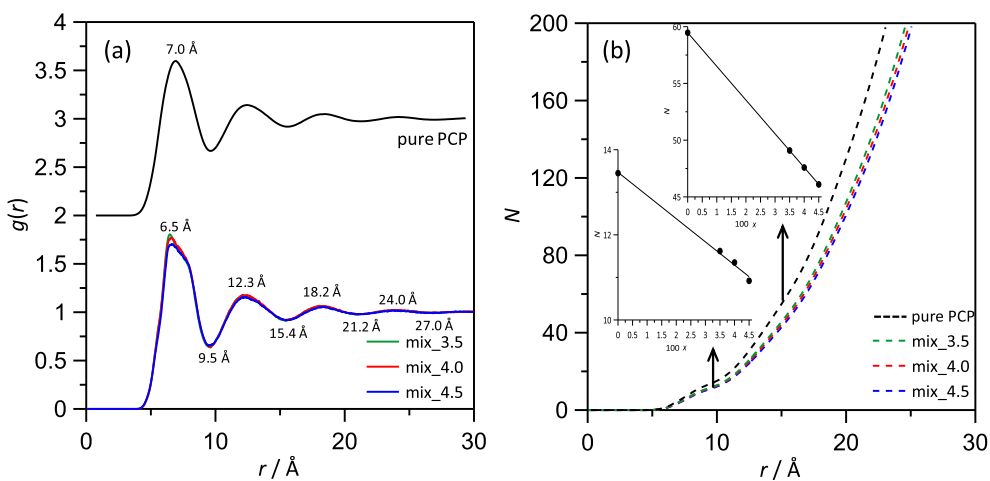

Fig. 7. (a) Center-of-mass – center-of-mass radial distribution function for PCP – PCP pairs and (b) the corresponding solvation numbers, N, for cage(3^3:13^3) + PCP solutions for different cage content from MD simulations at 300 K. The position of maxima and minima are reported in panel a; values for N in the first and second solvation shells are reported inside panel b. In panel b, x stands for cage(3^3:13^3) mole fraction.
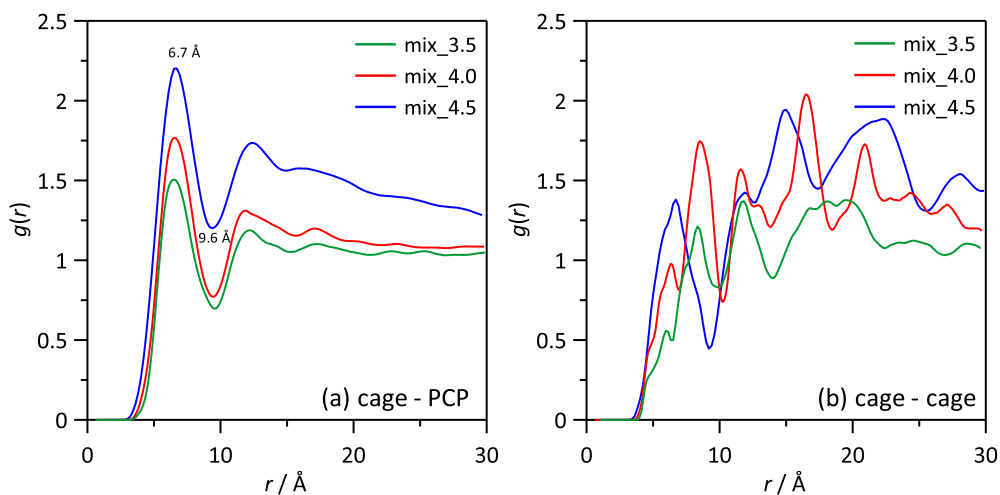

Fig. 8. Center-of-mass – center-of-mass radial distribution function for (a) cage – PCP and (b) cage – cage pairs, for cage(3^3:13^3) + PCP solutions for different cage content from MD simulations at 300 K. The position of maxima and minima are reported in panel a.
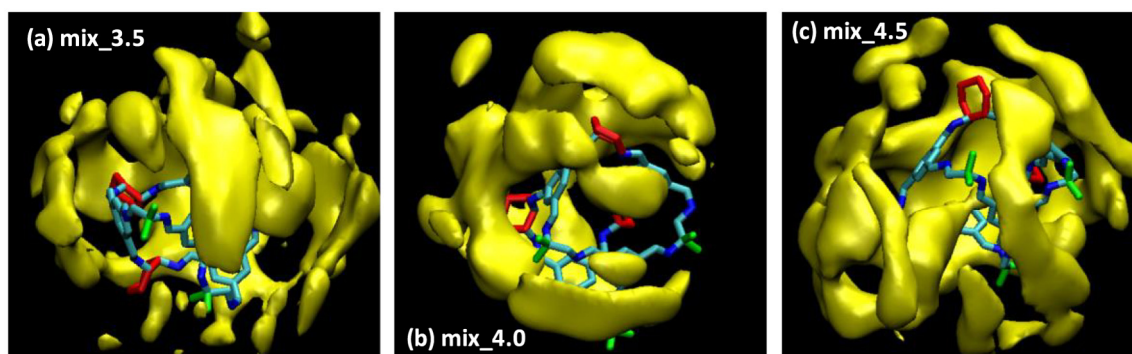
Fig. 9. Spatial distribution functions of PCP (yellow isosurfaces) around central cage(3^3:13^3) molecules for cage(3^3:13^3) + PCP solutions for different cage content from MD simulations at 300 K.

with neat solvent., Fig. 7a. Results show almost negligible changes because of the presence of cage molecules, the structure of RDFs is maintained in terms of main peaks positions and intensities and although some minor changes are inferred in some peaks, increasing with concentration, e.g. the first RDF peak, these RDFs support equivalent PCP structuring in neat PCP as well as in cage solutions. The first RDF peak at 6.5 Å evolves with the formation of a shoulder at roughly 8.5 Å when cage solutions are formed, which can be attributed to the self-interaction of PCP molecules in the region in the vicinity of the cage (cage windows or direct solvation, Fig. 6a). The integration of the RDFs led to the solvation numbers in Fig. 7b, which show a decrease with increasing cage concentration in an almost linear way. This effect may be again attributed to the local disruption of PCP molecules in the vicinity of the cages for proper cages solvation, with the cage to PCP interactions decreasing the PCP to PCP ones in the solvation shells around the cages.

The solutions structuring was also analysed considering RDFs for cage – PCP and cage – cage (center-of-mass) interactions, Fig. 8. The RDFs for cage – PCP interactions, Fig. 8a, are characterized by a first wide (from 4.5 to 9.6 Å) peak corresponding to molecules around the cage surface, involving both those in the cage windows as well as in the first solvation shell. This structuring for RDFs is maintained in the whole studied cage concentration range with no remarkable changes in the cage solvation for the studied concentration range. The

Fig. 10. Intermolecular interaction energy, E_{inter}, for cage(3^3:13^3) + PCP solutions for different cage content from MD simulations at 300 K.

distribution PCP molecules around cages is confirmed using the Spatial Distribution Functions, SDFs, reported in Fig. 9. First, the absence of PCPs inside the cavities is confirmed. Second, for lower cage concentrations, Fig. 9a, PCP concentrations around the cage windows are large, whereas when the PCP concentration increases, Fig. 9c, PCP molecules are more delocalized around the whole cage surface, which agrees with the increase of RDF peaks with cage concentration in Fig. 8a. For the case of cage – cage interactions, Fig. 8b, the reported RDFs show a certain degree of cage – self interaction, as confirmed by the first RDF peak in the 5 to 10 Å range increasing with cage concentration, thus although these results show mostly cages dispersed between the PCP solvent molecules, cage – cage self-interaction is also present in the solutions.

The strength of intermolecular interactions was calculated using the interaction energy, E_{inter}, for the involved molecular pairs, Fig. 10. First, results in Fig. 8b showed a certain cage self-interaction with the formation of cage – cage clusters, this is confirmed in Fig. 10 by the large values of E_{inter}, increasing with cage concentration in a linear way. Likewise, the E_{inter} for cage – cage interactions are remarkably larger than those for cage – PCP or PCP – PCP ones, which can be justified considering that all these interactions are of van der Waals nature, thus being dependent on the number of van der Waals contacts, i.e. interacting atomic pairs, which are remarkably larger for the bulky cages. The E_{inter} for PCP – cage interactions are only slightly lower than those for PCP – PCP interactions, and increase (in absolute value) with cage concentrations, in agreement with the larger number of PCP molecules in the first solvation shell around the cages, Fig. 8a. Likewise, E_{inter} for PCP – PCP interactions decreases (in absolute value) with increasing cage content, which agrees with the decrease in PCP – PCP interactions as inferred from RDFs in Fig. 7b. Nevertheless, this decrease in E_{inter} for PCP – PCP pairs is only very minor for the studied concentration range, thus confirming that although the trend of PCP molecules to effectively solvate cage molecules, which agrees with DFT results, decreases the PCP self-association, this effect is very minor, with the solvent maintaining most of its features even in presence of the bulky cage molecules.

The dynamic properties of the studied solutions were also analysed. Self-diffusion coefficients, D, were calculated from mean square displacements and Einstein's equation, Fig. 11a. The D values for PCP and cage molecules decrease with increasing concentration in an almost linear way, Fig. 11a, which leads to an increase of viscosity (calculated using Green-Kubo method), but in this case in a non-linear way, Fig. 11b. MD calculated values for cage molecules are slightly larger than experimental values reported in the literature [6], which leads to lower viscosities, Fig. 11b, but MD prediction can be considered in suitable agreement with experiments. Likewise, D values for PCP molecules are three fold larger than those for the cages, which may be justified considering on one side the larger size of cage molecule as well as the larger E_{inter} values for interactions involving cage molecules, Fig. 10. Regarding PCP mobility, the presence of cage molecules decreases D in
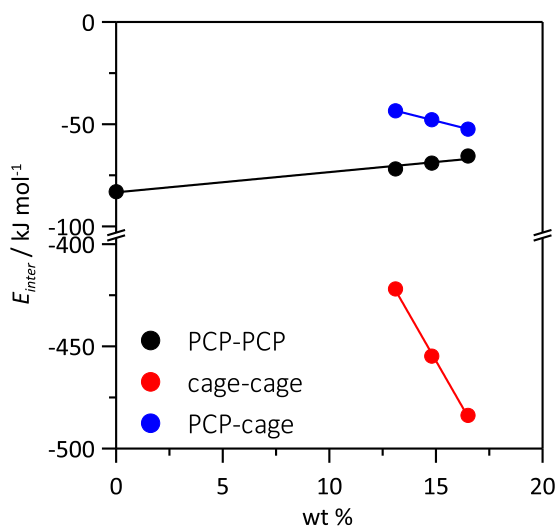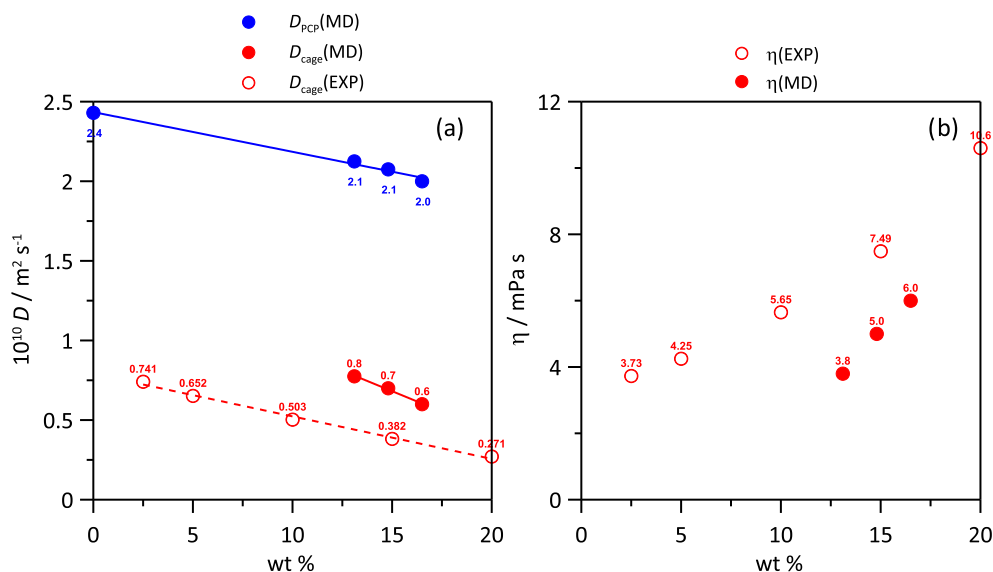
Fig. 11. (a) Center-of-mass self-diffusion coefficients, D (values for the cage and PCP molecules are reported), and (b) dynamic viscosity, for cage(3^3:13^3) or PCP molecules for cage(3^3:13^3) + PCP solutions for different cage content from MD simulations at 300 K. Experimental values from the literature [6] are reported for comparison purposes.

comparison with neat PCP solvent, but this decrease is very minor (from 2.4 to 2.0 10^{-10} m^2 s^{-1} in the studied concentration range), thus showing that although E_{inter} for cage – PCP interactions are large, Fig. 10, the effects of cage – PCP interactions are localized in the shell around the cage, RDFs in Fig. 8a, thus with minor disruption in bulk liquid PCP behaviour.

3.3. DFT results for molecular clusters cage + PCP + CO$_2$

The presence of cavities in the studied porous liquid makes this fluid a suitable material for CO$_2$ capturing purposes. To analyse the cage – CO$_2$ interactions 1:1 clusters were studied using DFT, including CO$_2$ molecules placed in the external surface of the cage (clusters 01 to 05), considering the sites with largest ΔE values, as well as inside the cage cavity (cluster 06), Fig. 12. The reported results show some variations but considerably large binding energies for all the arrangements of CO$_2$ molecule on the external surface of the cage, very effective interaction is inferred both for gas molecules placed on the cage windows as well as for the placement near de dimethyl sites. The confinement of CO$_2$ molecule leads to remarkably larger interaction energies than for any of the orientations outside of the cavity, thus the confinement is preferred to adsorption on the external surface, which would justify the trend of CO$_2$ molecules to penetrate into the cage internal cavity.

The large stabilization of CO$_2$ molecules upon confinement inside the cage is analysed in Fig. 13 using both AIM and NCI approaches. The CO$_2$ molecule inside the cage cavity leads to the formation of a massive number of RCPs and CCPs according to AIM approach, Fig. 13a, thus, showing how gas molecule may interact very effectively with all the surrounding atoms forming the cage cavity. The nature of the CO$_2$ molecule – cage interaction is determined using NCI method, Fig. 13b. The region surrounding the CO$_2$ molecule is characterized by a large surface showing van der Waals like interactions with all the surrounding cage atoms. Therefore, CO$_2$ molecule leads to large interaction energy through the simultaneous interaction with surrounding environment, which considering the size of CO$_2$ molecules leads to effective packing and van der Waals forces, thus favouring molecular confinement and confirming that the studied cage can be used for effectively storing CO$_2$ molecule. Likewise, the cage - CO$_2$ molecule interaction energy point to stabilization upon CO$_2$ confinement but it is not too large to allow desorption upon heating [31], thus favouring the use of these cages for CO$_2$ capturing purposes.
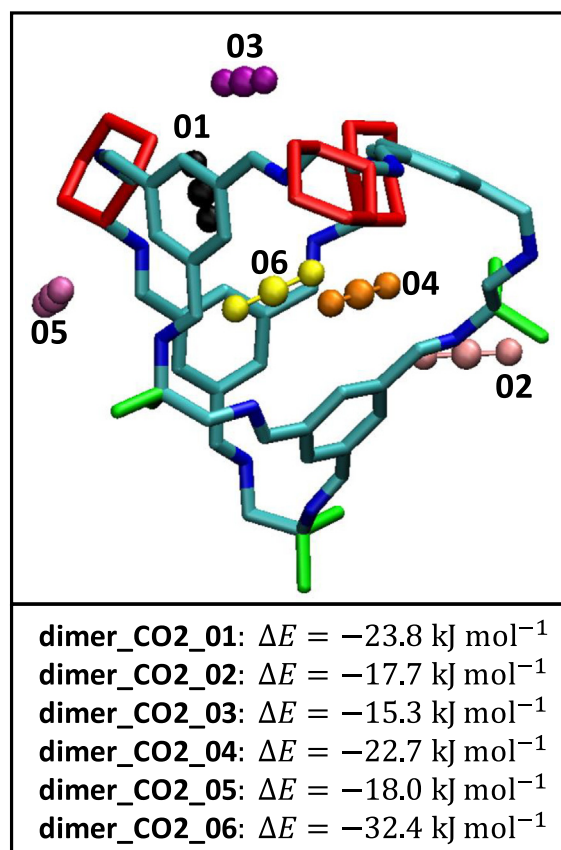

Fig. 12. Optimized structures of cage(3^3:13^3) – CO$_2$ dimers for different possible interaction sites, calculated at B3LYP / 6-311G(d,p) theoretical level. Counterpoise corrected interaction energies, ΔE, are reported for each dimer. Color code as in Fig. 1. CO$_2$ molecules are reported in different colors to highlight the studied sites. Position 06 shows CO$_2$ confined inside the cage cavity.
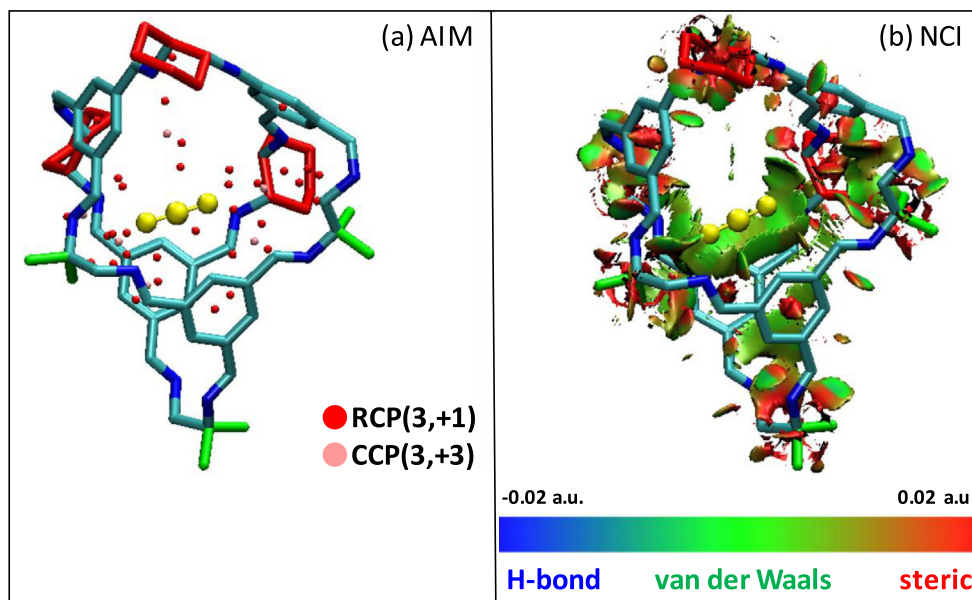
Fig. 13. (a) AIM and (b) NCI analysis of CO_2 molecule confined inside the cavity of cage(3^3:13^3) calculated at B3LYP / 6-311G(d,p) theoretical level.

3.4. MD results for CO_2 in cage + PCP liquid mixtures

The properties of CO_2 in PCP + cage solutions were firstly analysed using MD considering the percentage of cage occupancy, Fig. 14a. It is reported in the literature an average occupancy of 54% [6] and results reported in this work show a slightly lower average occupation (45.7%) at 300 K but in reasonable agreement. Thus, half of the cages are occupied at 300 K. It should be remarked that CO_2 molecules also show a relevant affinity for the external surface of the cages; thus molecules may be also stabilized when adsorbed on the cage surface, thus hindering their penetration toward the internal site. The dynamic picture of CO_2 molecules situation may be inferred from the time evolution of cage occupancy at isothermal conditions, Fig. 14a. The reported results show the although the cage occupancy remains close to the average value, there are several events of occupancy decrease or increase, i.e. a very dynamic behaviour is inferred with gas molecules leaving or penetrating the cage internal cavity, which can be justified considered the affinity of CO_2 molecules both for the internal cavity as well as for the cage surface. The MD interaction energy is reported inn Fig. 14b showing its dynamic behaviour. The energy for CO_2 – PCP interactions are three-times larger than for CO_2 – cage ones, which show that CO_2 molecules are also prone to interact with PCP solvent molecules. The event episodes of cage occupancy showed in Fig. 14a are accompanied by parallel variations in interaction energies. A decrease in cage occupancy is also accompanied by a decrease of cage - CO_2 interaction energy and an increase in PCP - CO_2 energy, and vice versa for increasing cage occupancy. The CO_2 molecules leaving cage cavities allow interaction both with the external cage surface as well as with the PCP solvent molecules, with both types of interactions being only slightly less strong than those when CO_2 molecules are confined. These interaction energy – related issues would justify that only half-of the cavities are occupied by confined CO_2 molecules.

The dynamic properties of CO_2 – PCP – cage solutions were also studied considering the self-diffusion coefficients, Fig. 15a and compared with those for the solution in absence of CO_2 molecules. The absorption of CO_2 molecules leads to an increase of molecular mobility, the D values for PCP increases a 20% and for the cage a 14% is inferred. Thus, a disruptive effect is inferred because of the presence of CO_2 molecules, which can be justified by the formation of PCP - CO_2 interactions weakening PCP – PCP ones and thus leading to a decrease in fluid's cohesion
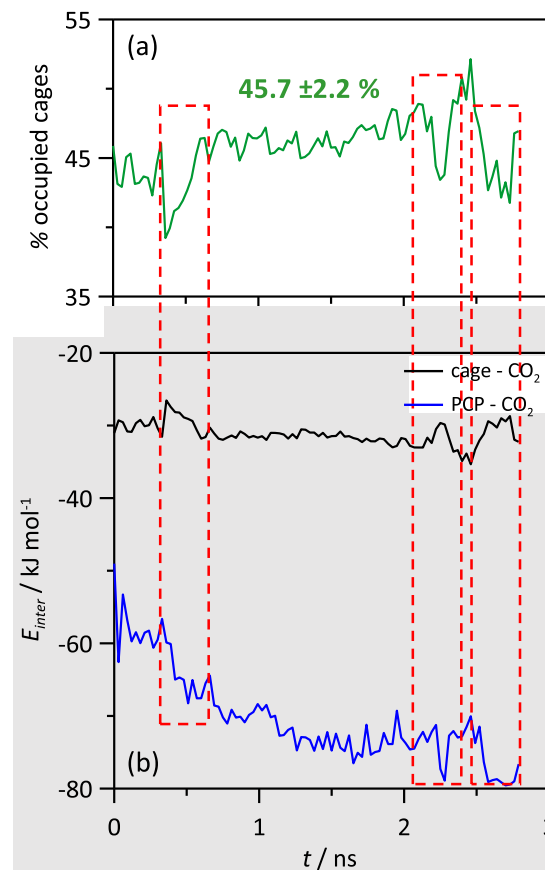

Fig. 14. (a) Percentage of occupied cages and (b) intermolecular interaction energy, E_{inter}, for the reported pairs in cage(3^3:13^3) + PCP + CO_2 solutions from MD simulations at 300 K. In panel a, the average occupancy is reported. Red dashed lines show correlated behaviour of occupancy and E_{inter}.
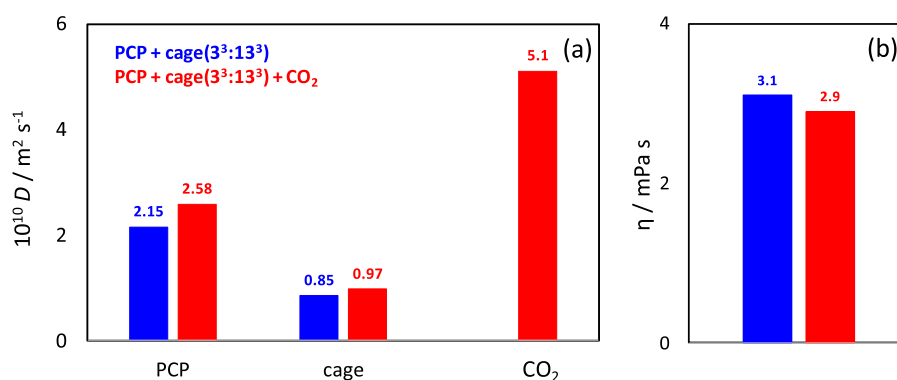
Fig. 15. (a) Self-diffusion coefficients, D, and (b) dynamic viscosity, η, for cage(3^3:13^3) + PCP and in cage(3^3:13^3) + PCP + CO_2 solutions.

favouring molecular mobility. Likewise, D values for CO_2 molecules are larger than for the PCP solvent or the cage. The increase in D values upon CO_2 absorption leads to a decrease (-6.4%) in the calculated dynamic viscosity. Nevertheless, it should be remarked that these solutions, porous liquids, are low viscous fluids, in absence or presence of CO_2, which would favour their application for carbon capturing,

favouring mass and heat transfer processes. Considering that CO_2 absorption – desorption processes may be developed at different temperatures for developing carbon capture operations, the behaviour of CO_2 - PCP – cage solutions was studied in the 300 to 340 K range, Fig. 16. The D values as a function of temperature are reported in Fig. 16a confirming an increase in molecular mobility for the three involved types of molecules, although the ordering CO_2 > PCP > cage is maintained in the studied temperature range. This increase in D values leads to a remarkable non-linear decrease in viscosity, Fig. 16b, reaching a very low value (1.1 mPa s) at 340 K, which show a suitable increase in fluidity at moderate temperatures. Nevertheless, in spite of the increase in molecular mobility the percentage of cages occupancies only decreases (on average) from 45.7% at 300 K to 40% at 340 K, thus confirming the large affinity of CO_2 molecules for the cage cavity even at moderate temperatures and showing the suitability of the studied porous solvent for the development of carbon capture operations.

4. Conclusions

The properties of cage (3^3:13^3) cage in liquid perchloropropene (PCP) are studied using a computational approach considering quantum chemistry and molecular dynamics. The type II porous liquid character is confirmed by the absence of solvent molecules inside the cavity for the studied concentration ranges. PCP molecules are able to efficiently solvate cage molecules, with minor fluid's disruption, with the solvent molecules placed around the cage windows and in a first solvation shell around the cages. The interaction of solvent molecules with cages are of van der Waals nature but leading to very efficient interactions with minor disruptions of solvent self-association. Likewise, cages are able to self-interact contributing to fluids' stabilization.

The absorption of CO_2 molecules is favoured by a stabilization of gas molecules confined inside the cage cavities but also because of suitable interaction with cage external surfaces and with the solvent molecules, which leads to half of the cage cavities occupied but with a dynamic behaviour characterized by molecules leaving and entering the cage. The confined CO_2 molecules leads to very efficient van der Waals interactions with the surrounding environment, favouring stabilization upon confinement. The cages occupancy is maintained in the 300 to 340 K temperature range, which provides a suitable window for using these liquid materials for CO_2 absorption. The considered porous liquid is moderately viscous with the viscosity decreasing to low values upon gas adsorption, which would favour its applicability at industrial scale. Therefore, the considered porous liquid is able to admit cages in a suitable concentration range without large changes in the solvent properties but leading to a type II porous material with cages suitable to capture CO_2 because of the large affinity for the cages both for the solvent and the adsorbed gas molecules.
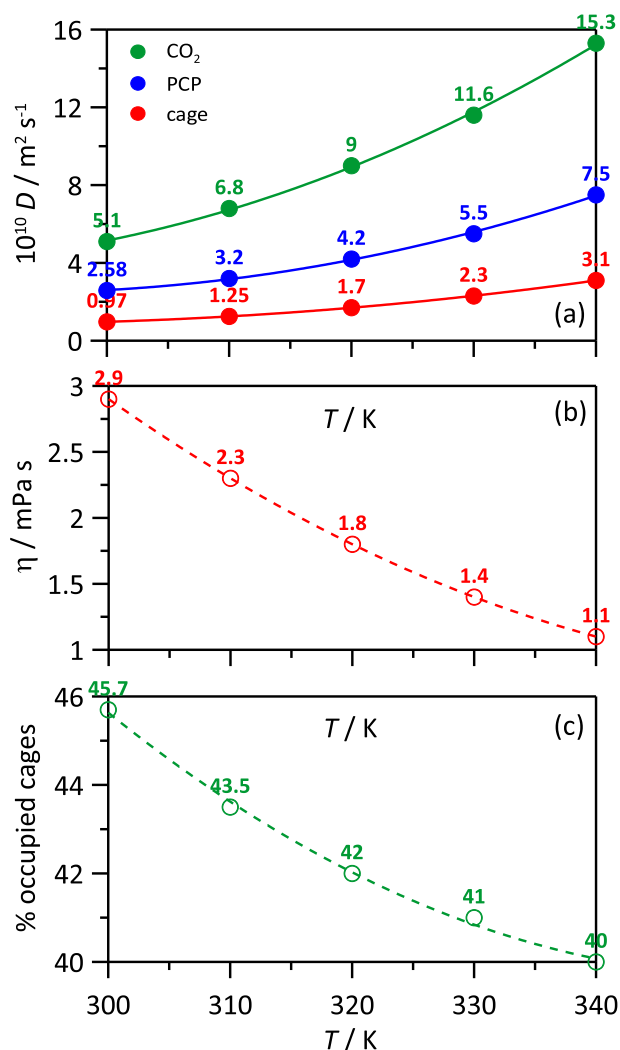

Fig. 16. (a) Self-diffusion coefficients, D, (b) dynamic viscosity, η, and (c) percentage of occupied cages for cage(3^3:13^3) + PCP + CO_2 solutions as a function of temperature, T.

Declaration of Competing Interest

The authors whose names are listed immediately below certify that they have NO affiliations with or involvement in any organization or entity with any financial interest (such as honoraria; educational grants; participation in speakers' bureaus; membership, employment, consultancies, stock ownership, or other equity interest; and expert testimony or patent-licensing arrangements), or non-financial interest (such as personal or professional relationships, affiliations, knowledge or beliefs) in the subject matter or materials discussed in this manuscript.

Acknowledgements

Appendix A. Supplementary data

Supplementary data to this article can be found online at https://doi.org/10.1016/j.molliq.2021.115660.

References

[1] N. O'Reilly, N. Giri, S.L. James, Porous liquids, Chem. Eur. J. 13 (2007) 3020–3025.
[2] A. Bavykina, A. Cadiau, J. Gascon, Porous liquids based on porous cages, metal organic frameworks and metal organic polyhedral, Chem. Coord. Rev. 386 (2019) 85–95.
[3] R.J. Kearsey, B.M. Alston, M.E. Briggs, R.L. Greenaway, A.I. Cooper, Accelerated robotic discovery of type ii porous liquids, Chem. Sci. 10 (2019) 9454–9465.
[4] T. Tozawa, J.T.A. Jones, S.I. Swamy, S. Jiang, D.J. Adams, S. Shakespeare, R. Clowes, D. Bradshaw, T. Hasell, S.Y. Chong, C. Tang, S. Thompson, J. Parker, A. Trewin, J. Bacsa, A.M.Z. Slawin, A. Steiner, A.I. Cooper, Porous organic cages, Nat. Mater. 8 (2009) 973–978.
[5] N. Giri, M.G. Del Pópolo, G. Melaugh, R.L. Greenaway, K. Rätzke, T. Koschine, L. Pison, M.F.C. Gomes, A.I. Cooper, S.L. James, Liquids with permanent porosity, Nature 527 (2015) 216–220.
[6] R.L. Greenaway, D. Holden, E.G.B. Eden, A. Stephenson, C.W. Yong, M.J. Bennison, T. Hasell, M.E. Briggs, S.L. James, A.I. Cooper, Understanding gas capacity, guest selectivity, and diffusion in porous liquids, Chem. Sci. 8 (2017) 2640–2651.
[7] B.E. Egleston, K.-V. Luzyamin, M.C. Brand, R. Clowes, M.E. Briggs, R.L. Greenaway, A.I. Cooper, Controlling gas selectivity in molecular porous liquids by tuning the cage windo size, Angew. Chem. Int. Ed. 132 (2020) 7432–7436.
[8] J. Zhang, N. Lv, Y. Chao, I. Chen, W. Fu, J. Yin, H. Li, W. Zhu, H. Li, The interaction nature between hollow silica-based porous ionic liquids and CO$_2$: A DFT study, J. Mol. Graph. Model. 100 (2020) (107694).
[9] J. Yi, W. Fu, J. Zhang, H. Ran, N. Lv, Y. Chao, H. Li, W. Zhu, H. Liu, H. Li, Unraveling the mechanism of CO$_2$ capture and separation by porous liquids, RSC Adv. 10 (2020) 42706–42717.
[10] J. Yin, J. Zhang, W. Fu, D. Jiang, N. Lv, H. Liu, W. Zhu, Theoretical prediction of the SO$_2$ absorption by hollow silica based porous ionic liquids, J. Mol. Graph. Model. 103 (2021) 107788.
[11] F. Neese, The ORCA program system, WIREs Comput. Mol. Sci. 2 (2012) 73–78.
[12] C. Lee, W. Yang, R.G. Parr, Development of the Colle-Salvetti correlation-energy formula into a functional of the electron density, Phys. Rev. B 37 (1988) 785–789.
[13] A.D. Becke, Density-functional exchange-energy approximation with correct asymptotic behavior, Phys. Rev. A 38 (1988) 3098–3100.
[14] S. Grimme, J. Antony, S. Ehrlich, H.A. Krieg, Consistent and accurate ab initio parametrization of density functional dispersion correction [DFT-D] for the 94 elements H-Pu, J. Chem. Phys. 132 (2010) 154104.
[15] S. Simon, M. Duran, J.J. Dannenberg, How does basis set superposition error change the potential surfaces for hydrogen-bonded dimers? J. Chem. Phys. 105 (1996) 11024–11031.
[16] C.M. Breneman, K.B. Wiberg, Determining atom-centered monopoles from molecular electrostatic potentials. The need for high sampling density in formamide conformational analysis, J. Comput. Chem. 11 (1990) 361–373.
[17] R.F.W. Bader, Atoms in Molecules: A Quantum Theory, Oxford University Press, 1990.
[18] T. Lu, F. Chen, Multiwfn: a multifunctional wavefunction analyzer, J. Comput. Chem. 33 (2012) 580–592.
[19] S. Aparicio, C.T. Yavuz, M. Atilhan, Molecular insights into benzimidazole-linked polymer interactions with carbon dioxide and nitrogen, ChemistrySelect 3 (2018) 3691–3701.
[20] J. Xiao, Y.P. Zhao, X. Fan, J.P. Cao, G.J. Kang, W. Zhao, X.Y. Wei, Hydrogen bonding interactions between the organic oxygen/nitrogen monomers of lignite and water molecules: a DFT and AIM study, Fuel Process. Technol. 168 (2017) 58–64.
[21] V. Anbu, K.A. Vijayalakshmi, R. Karunathan, A.D. Stephen, P.V. Nidhin, Explosives properties of high energetic trinitrophenyl nitramide molecules: a DFT and AIM analysis, Arab. J. Chem. 12 (2019) 621–632.
[22] E.R. Johnson, S. Keinan, P. Mori-Sanchez, J. Contreras-García, A.J. Cohen, W. Yang, Revealing non-covalent interactions, J. Am. Chem. Soc. 132 (2010) 6498–6506.
[23] A.P. Lyubartsev, A. Laaksonen, MDynaMix - a scalable portable parallel MD simulation package for arbitrary molecular mixtures, Comput. Phys. Commun. 128 (2000) 565–589.
[24] V. Zoete, M.A. Cuendet, A. Grosdidier, O. Michielin, SwissParam, a fast force field generation tool for small organic molecules, J. Comput. Chem. 32 (2011) 2359–2368.
[25] T.A. Halgren, Merck molecular force field. I. Basis, form, scope, parameterization, and performance of MMFF94, J. Comput. Chem. 17 (1996) 490–519.
[26] L. Martínez, R. Andrade, E.G. Birgin, J.M. Martínez, Packmol: a package for building initial configurations for molecular dynamics simulations, J. Comput. Chem. 30 (2009) 2157–2164.
[27] U.L. Essmann, M.L. Perera, T. Berkowitz, H. Darden, H. Lee, L.G. Pedersen, A smooth particle mesh ewald method, J. Chem. Phys. 103 (1995) 8577–8593.
[28] M. Tuckerman, B.J. Berne, G.J. Martyna, Reversible multiple time scale molecular dynamics, J. Chem. Phys. 97 (1992) 1990–2001.
[29] W. Humphrey, A. Dalke, K. Schulten, VMD - visual molecular dynamics, J. Mol. Graph. 14 (1996) 33–38.
[30] M. Brehm, B. Kirchner, TRAVIS - a free analyzer and visualizer for Monte Carlo and molecular dynamics trajectories, J. Chem. Inf. Model. 51 (2011) 2007–2023.
[31] X. Li, S. Wang, C. Chen, Experimental study of energy requirement of CO$_2$ desorption from rich solvent, Energy Procedia 37 (2013) 1836–1843.